CHAPTER 5:
CHARGE INJECTION STUDIES

5.1 Introduction

As mentioned in chapter 4, the drift velocity of the electrons inside the silicon (v_{drift}) is temperature dependent thus, the detector's position resolution is affected by temperature variations. Hence, to preserve the high position resolution achievable with this detector it becomes desirable to have on-line calibration of the drift velocity.

Calibration of the drift velocity can be accomplished by injecting electrons through electrodes located at known positions and subsequently measuring the drift time of the electrons to the anodes [ref. 3.16, 5.1]. The injected electrons will follow the same path to the anodes as electrons liberated by ionizing particles. Therefore, charge injectors provide a very practical and accurate method for monitoring and calibrating the drift velocity of electrons.

Figure 5.1 shows the potential distribution near the surface of the detector, in the gap between two cathodes. Due to the positive charges fixed at the Si-SiO_2 interface, the potential between the two cathodes becomes more positive, producing a local potential well. This well extends from the surface up to a saddle point within the silicon bulk (a negative potential maximum), and is partially filled by electrons. The number of electrons accumulated in this potential well is the result of the dynamic equilibrium between the number of electrons generated in the bulk and at the surface and the number of electrons that escape past the saddle point, into the bulk or sideways along the cathode lines towards the guard regions

of the detector. The charge injection mechanism works by disturbing this equilibrium and causing the accumulated electrons to cross over the saddle point and flow into the bulk of the detector. The equilibrium is disturbed by pulsing a fast signal into the injector electrode placed in the gap between two cathodes. The injected pulse will change the potential at the surface for the duration of the pulse, as the electrons will be forced to pass through the saddle point into the detector bulk. Once the excess electrons are injected into the main valley across the saddle point, the equilibrium is restored.

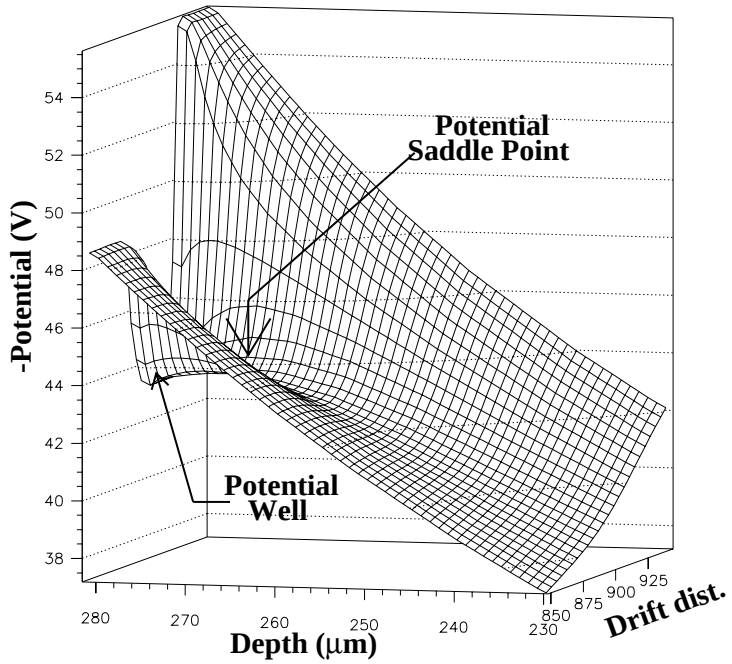

Figure 5.1: *Potential distribution near an injection line.*

5.2 MOS and Implanted type of injectors

Two types of injectors were implemented to be studied for the in the SDD's: implanted and MOS injectors (Metal-Oxide-Semiconductor). Figure 5.2 shows a schematic cross section of both types. The injector lines are positioned between two *'p+'* cathode strips and extend across the whole *6 cm* detector length. A total of eight (8) injection lines are implemented in each detector, four (4) on

each drift side. They are placed at approximate distances of *0.22 cm*, *1.0 cm*, *2.0 cm* and *3.0 cm* from the anodes.

The MOS injector consists of a continuous Aluminum line (≈*8 μm* wide) over a *3,500 angstrom* thick layer of SiO_2, placed between the cathode strips. In this case, the Aluminum electrode forms a capacitive contact with the silicon surface, underneath the oxide layer. MOS charge injectors are more commonly used and detailed information of previous tests can be found in reference 3.16 and 5.1.

The implanted injectors make a direct ohmic contact (as opposed to a capacitive contact) with the n-material of the bulk. The *n+* phosphorous implant increases the concentration of electrons accumulated at the surface, in the potential well. The implanted line also has a width of approximately *8 μm* with an Aluminum overlay for better electric contact.

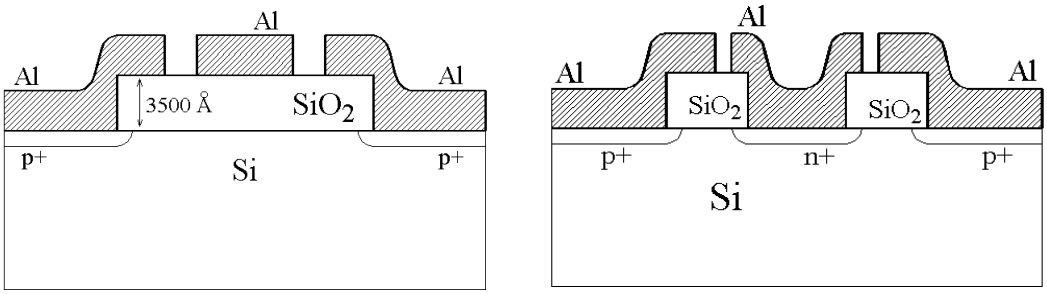

Figure 5.2: *Schematic cross section of the injector two types of injector structures implemented in the STAR SDD detectors: implanted and MOS injectors.*

Both injector types were connected to an external pulse generator through a capacitor. This capacitor (*3 kV, 2.2 nF)* is used to balance the potential difference between the injector line and the pulse generator that is kept at ground level. The rise time of the pulse which is lower than *10 ns*, is sufficiently fast compared to

the RC time constant of the injector capacitance, so that for the duration of the pulse, the local potential is affected directly by the input pulse.

In the following sections, I present results from several tests performed with both types of injectors and compare their performance.

5.3 Natural potential and the DC bias dependence.

Figure 5.1 showed the potential distribution near the surface, at the gap, between two cathodes. A local potential well is created by positive charges trapped at the $Si\text{-}SiO_2$ interface. Because the injector electrodes are floating, without a direct electric connection to the neighboring cathodes, they rest at a potential determined by the distribution shown in figure 5.1. This potential is defined as the '*natural*' potential of the injector line. In addition, the average bias value of the two neighboring cathodes is defined as '*mean-surface-bias*'. The natural potential of the injector was found to be around *15 V* less negative than the mean-surface-bias. The exact difference between the natural potential and the mean-surface-bias varies slightly from detector to detector due to its dependence on the density of fixed oxide charges.

By displacing the injector potential from its natural value, it is possible to change the behavior of injection characteristics. Figures 5.3a and 5.3b show the integrated signal at the anode as a function of the input pulse amplitude, for an implanted and a MOS injector type, respectively. The three different curves in each plot correspond to three different DC bias conditions for the injector line. The curve with solid circles corresponds to the measurements with the detector at its natural potential. For the curve with the solid squares, the injector was at a potential *6 V* less negative than the natural potential. Under this condition the injector is considered to be 'under-biased'. The curve with the open squares is for

the case when the injector is ‘over-biased’, *4 V* more negative than the natural potential value.

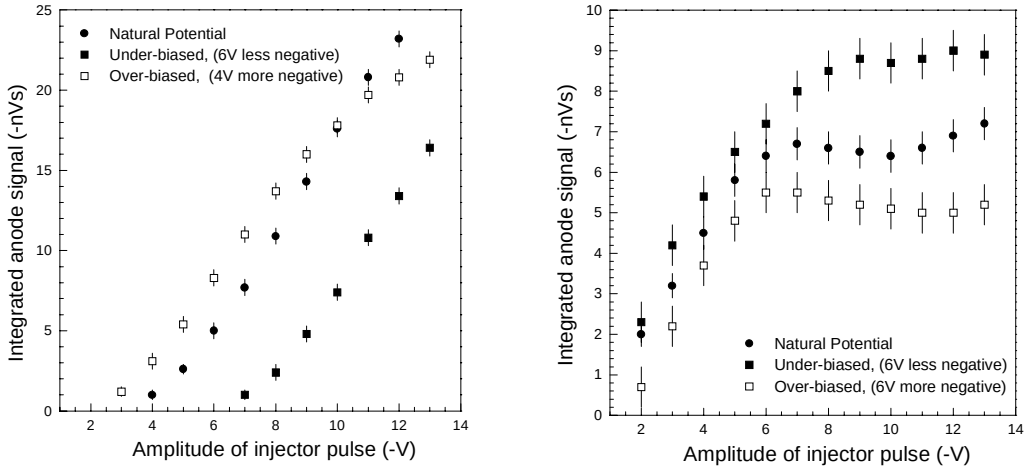

(a) from implanted injector **(b) from MOS injector**

Figure 5.3*: Integrated signal measured at the anode as a function of input pulse amplitude, for (a) an implanted type injector and (b) a MOS type injector.*

For the implanted injector (figure 5.3a), the measured signal increases monotonically with the amplitude of the injection. Notice the threshold effect as a function of injector DC bias. With the injector over-biased, a lower amplitude is necessary to start injecting. In figure 5.3b, the MOS injector shows a much smaller dependency on the DC bias variation. Also, the integrated signal from the MOS injector saturates and stays independent of any further increase of the input amplitude. To better understand the difference between the two types of injectors, simulation studies for the potential distribution in the injector region were performed utilizing the same simulation package used to calculate the potential distribution near the anodes, see chapter 02. [ref. 3.14]

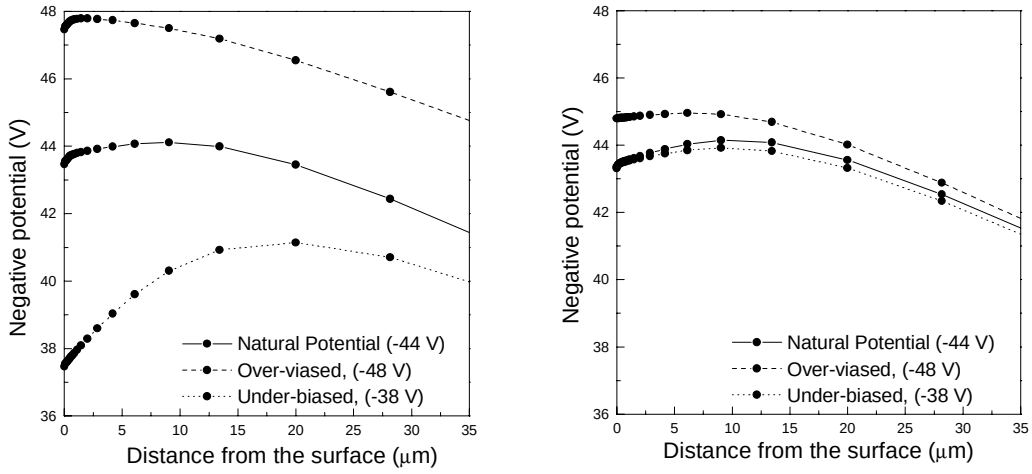

(a) Implanted injector **(b) MOS injector**

Figure 5.4: *Negative potential underneath the injector line, as a function of the distance from the surface of the detector towards the center of the bulk for the case of (a) the implanted type injector and (b) the MOS type injector.*

Figures 5.4a and 5.4b show the potential distribution in the silicon, from the surface towards the center of the detector bulk, for the implanted and the MOS injector types, respectively. The solid curves correspond to the potential distribution with the injectors at their natural potential. The dashed and the dotted curves correspond to the over-biased condition (*4 V* more negative) and under-biased condition (*10 V* less negative), respectively.

The strong dependency of the implanted injector on the DC bias can be understood by correlating the plots 5.3a and 5.4a. In the natural potential condition, the electrons trapped in the potential well have to overcome a barrier to flow into the center of the detector. Increasing the input pulse amplitude increases the amount of electrons that will be pushed across the saddle point into the bulk. Therefore, the signal from the injector increases with the input pulse amplitude as seen in figure 5.3a. When the DC bias is varied, due to the direct ohmic contact, the potential value in the silicon changes accordingly. When the injector is under-

biased, the potential barrier increases, and a higher input pulse is required to inject electrons. Increasing the DC bias (towards more negative values) reduces the potential barrier and consequently a lower input amplitude is necessary to inject.

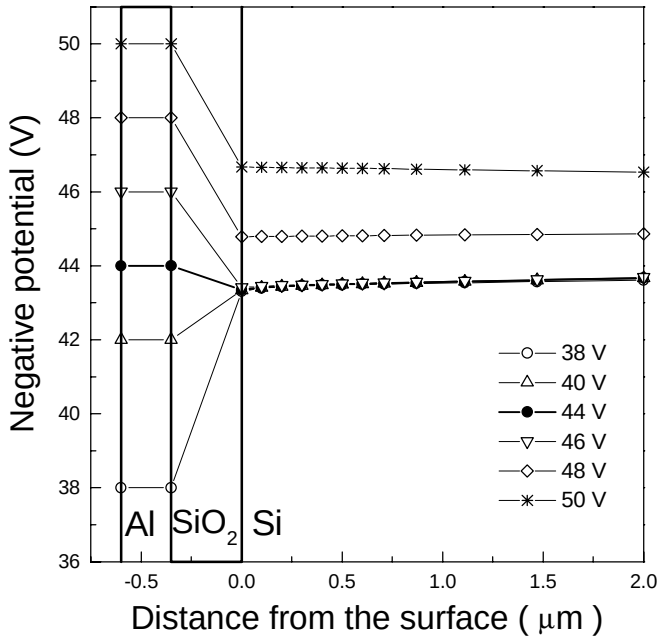

Figure 5.5: *Negative potential underneath the MOS injector for different bias conditions.*

The MOS injector has a smaller dependency on the DC bias. Figure 5.5 shows the potential distribution near the MOS injector, on a larger scale, including the SiO_2 layer and the Aluminum layer. Due to the capacitive nature of the SiO_2, the potential in the silicon remains unchanged, while the voltage difference takes place in the SiO_2. However, increasing the DC bias (towards more negative values) depletes the electrons that were accumulated near the silicon surface in the potential well. In figure 5.3b, for low input injection pulse, increasing the amplitude increases the measured output signal. More electrons are injected past the saddle point. The injection reaches a saturation point when the input pulse height is large enough to disturb the potential above the saddle point and all the

electrons originally trapped at the potential well are pushed into the detector. For the MOS injector, the saturation value depends on the amount of electrons initially trapped in the potential well, and therefore depends on the DC bias of the injector.

To characterize this effect, we show the amplitude of the input pulse necessary to measure a fixed integrated output signal, as a function of the injector DC bias (figure 5.6). The value of the fixed integrated output was chosen to be considerably small ($\approx 5nVs$), so that the curve in figure 5.6 represents approximately the threshold amplitude for injection. The DC bias, plotted on the '*x*' axis, is referenced with respect to the natural potential of the injector. The curve with open squares corresponds to the measurements from the implanted injector. The solid circles correspond to the equivalent measurement from the MOS injector.

As expected, by increasing the DC bias of the implanted injector, the input amplitude necessary to inject reduces, therefore, injection becomes easier. The injection improves up to a critical point, which corresponds to the minimum of the curve in figure 5.6, around $5\ V$ more negative than the natural potential. Above this point, there is a considerable increase of the current flow into the bulk, which causes a distortion of the potential distribution and the injection signal can no longer be measured in the anodes. Under this condition, the potential distribution near the surface of the implanted injector is high enough for the potential well to disappear and the electrons from the $n+$ implant flow freely into the detector bulk.

The MOS injector depends much less on the DC bias variation, as was expected from the simulation. The MOS injector performs efficiently near its natural potential condition. This is in agreement with the results shown in figures 5.3b and 5.4b. Similar to the implanted injector, a threshold value is observed for the DC bias, above which no injection can be measured. This threshold value is caused by the depletion of the accumulated electrons originally trapped in the potential well due to the high DC bias applied to the MOS capacitor.

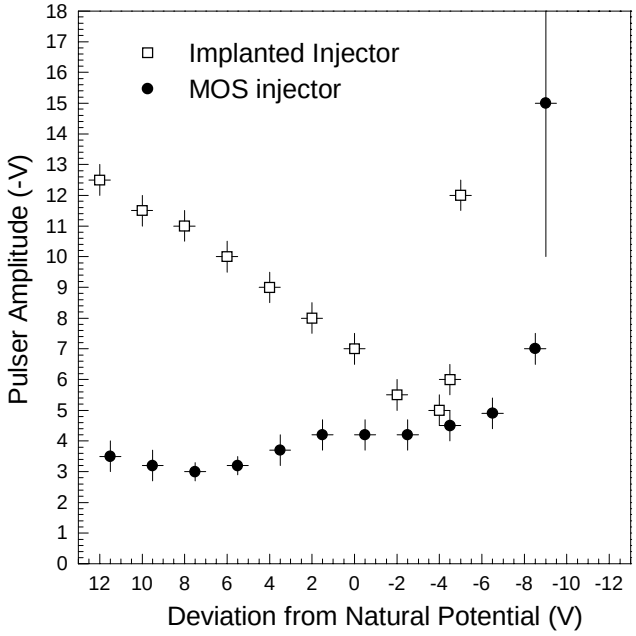

Figure 5.6: *Input pulse amplitude required to produce a fixed size anode signal as a function of DC bias for MOS injector (solid circles) and implanted injector (open squares).*

Figure 5.6 summarizes the injection dependence on the DC bias. With the implanted injector, it is possible to have better control of the injected charge, by controlling the DC bias. But changing the DC bias can also affect the leakage current that flows into the bulk. Thus, an important advantage of the MOS injector is that it does not introduce any additional leakage current to the bulk.

5.4 Lateral uniformity of injectors

If the number of electrons injected into the detector from a line injector were reproducible and uniform across the detector, then charge injection could also be used to monitor the relative gain between readout channels and provide an absolute calibration for each anode. Figure 5.7 shows the integrated anode signal from two injection lines, for every third anode, as a function of anode number. The

same pre-amplifier and signal shaper were used to measure the anode signal, therefore the variations in the collected charge is due to either relative collection efficiency of the anodes or injection non-uniformity. The open circles correspond to the integrated anode signal when pulsing the second implanted injector (at *1.0 cm* away from the anodes) and the open squares represent the equivalent measurement when pulsing the third injector line (positioned at *2.0 cm* from the anodes), also an implanted injector line. The relative variation between the two curves indicates that the non-uniformity is not due to anode collection efficiency but rather to the injectors themselves. The MOS injectors were also tested and show similar non-uniformities.

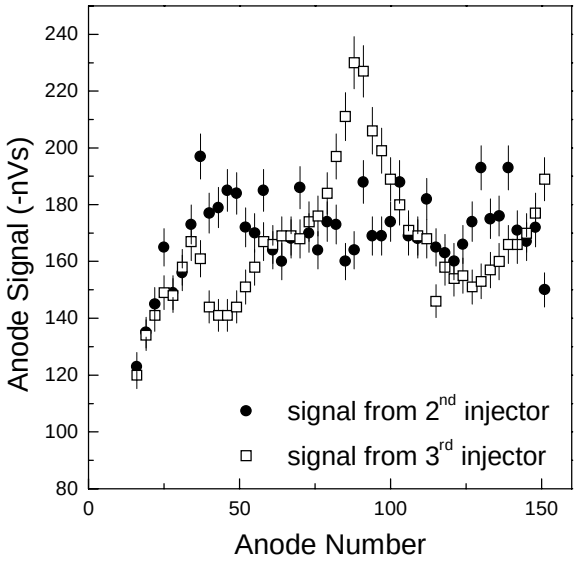

Figure 5.7*: Comparison of the integrated anode signals from Implanted injectors at one centimeter (solid circles) and two centimeters (open squares).*

The non-uniformity varies from detector to detector and with different injection parameters, for example DC bias and input pulse amplitude. Since the factors governing the injection amplitude and uniformity are most likely subject to uncontrolled variations such as oxide charge distribution and temperature

variations across the detector, it presently appears impractical to use injectors for gain calibration purposes. However, the relative gain between anodes is a fixed parameter, and it can be measured and mapped by other methods, such as laser injection.

5.5 The dot injector

The dot injector line consists of a series of small ($4\times20\ \mu m^2$) implants connected by an Aluminum overlay. With these implanted dots, it is possible to inject electrons at discrete points. A magnetic field with a component perpendicular to the drift direction and to the detector surface can cause a lateral shift of the electron cloud (Hall effect, see section 7.2.1). With the dot injectors, it is theoretically possible to measure this lateral shift.

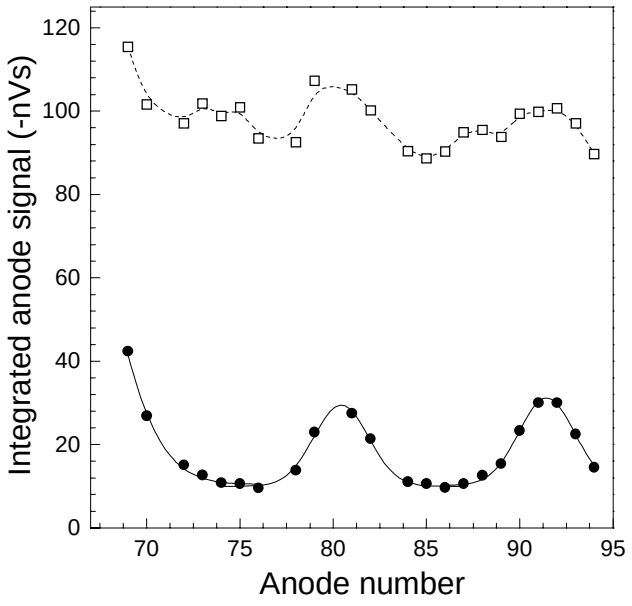

Figure 5.8: *Injection signal from a dot injection line for two different DC bias configurations.*

Figure 5.8 shows the integrated signal measured over a series of consecutive anodes when pulsing the dot injector line. These measurements were performed with the detector on a testing bench without any magnetic field. The anodes aligned with the position of the dot injectors measure a higher signal as shown by the solid line. However, anodes that are not directly aligned with the dot injectors also measure some signal. Part of this signal can be attributed to the charge spread from the dot injector, but part of the signal is due to MOS type injection from the metal overlay that connects the implanted injectors. In the previous sections, it was shown that both injection mechanisms depend differently on external DC bias conditions. By adjusting the DC bias, it is possible to enhance one type of injection mechanism over the other. For example, by "over-biasing" (more negative than the natural potential) the implanted injection is favored over the MOS injection, which subsequently leads to enhanced dot injection. On the other hand, by keeping the injection line at its natural potential, and using a relatively small injection pulse ($<5V$), the MOS injection mechanism has a better efficiency over the implanted injection, and a line structure is measured instead of the discrete dot structure. The second curve in figure 5.8 (dashed with open squares) shows the integrated signal measured with the same anodes, and pulsing the same dot injector line, but with a different DC bias.

Figure 5.9 shows for a different detector, a two-dimensional plot of the integrated anode signal amplitude versus drift time for a series of anodes for dot injector pulsing. The time axis shows the time distribution of the injected signal in time steps (buckets) of *40 ns*. The electronics used for this measurement is similar to that of STAR, and will be described in detail in chapter 06. The signal peaks are quite well separated and any shift in the lateral direction due to a magnetic field can be easily detected.

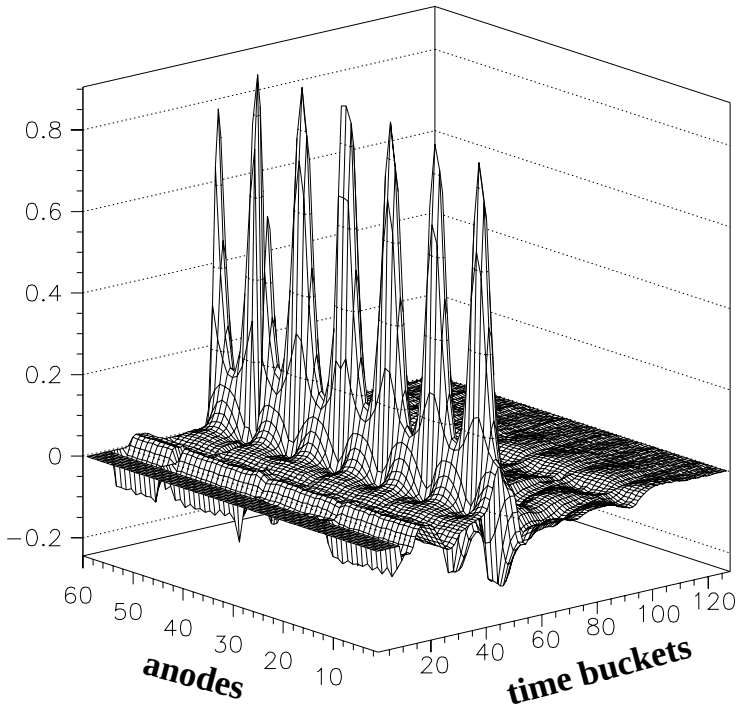

Figure 5.9: *Signal amplitude as a function of drift time and anode number for injection from a dot line structure.*

Dot injectors are certainly useful for the reasons mentioned earlier. However, to obtain an efficient dot injection, it is necessary to keep the injection line over-biased, which also increases the amount of leakage current injected into the detector bulk.

5.6 Summary of injection studies and suggestion for future possibilities

During the experiment, charge injection events will be interlaced with the real events to calibrate the drift velocity as a function of temperature variations in time. To be practical, charge injection must be simple and reproducible. With both types of injection mechanisms (implanted and MOS), the time calibration response has proven to be adequate.

Implanted charge injection is most efficient when biased more negatively than its natural potential. That can be accomplished in a simple manner, by attaching electrically the injection line to a neighboring cathode through a high value resistor. However, the implanted line is a direct connection to the detector bulk and undesirable surface currents can leak through the implanted lines into the bulk and to the anodes. In addition, the extra-bias of the injectors also contributes to the current increase. For those reasons, it was decided not to use implanted injection lines in the final version of the STAR/SVT drift detector [ref. 3.17].

MOS injectors have shown to perform adequately under normal bias conditions. Due to the fact that the injection line is not directly connected to the detector bulk, it does not affect the bulk current. Therefore, MOS type injectors are preferred over implanted structures. In the final design, the STAR/SVT Silicon Drift Detectors are instrumented with MOS type injection lines.

Based on our detailed charge injection studies, we propose a new type of charge injection mechanism for the future, namely a hybrid mechanism between the two types of injectors studied. It consists of a MOS line, with a smaller thickness of SiO_2 (~ 1000 Å), in addition to a donor $n+$ implantation underneath the oxide. The implantation increases the charge density underneath the injection line, and therefore enhances the injection magnitude, while the MOS nature of the structure avoids the surface currents to leak into the bulk though the injector. This new type of injection mechanism was implemented into a small scale test drift device, based on a design similar to the STAR detector. Several detectors of this kind were produced at BNL and are being tested. It is expected that the hybrid injection mechanism will improve the efficiency of charge injection considerably, making it more reliable for application in future Silicon Drift Detectors.